Addressing molecular geometry on dense gold nanoparticle substrates by two-color sum-frequency generation spectroscopy combined with DFT calculations

Grégory Barbillon, Christophe Humbert, Carine Clavaguéra, Audrey Gayral, Lidia Martínez, Yves Huttel, José Miguel García-Martín

Graphical Abstract

Addressing molecular geometry on dense gold nanoparticle substrates by two-colour sum-frequency generation spectroscopy combined with DFT calculations

Grégory Barbillon, Christophe Humbert, Carine Clavaguéra, Audrey Gayral, Lidia Martínez, Yves Huttel, José Miguel García-Martín

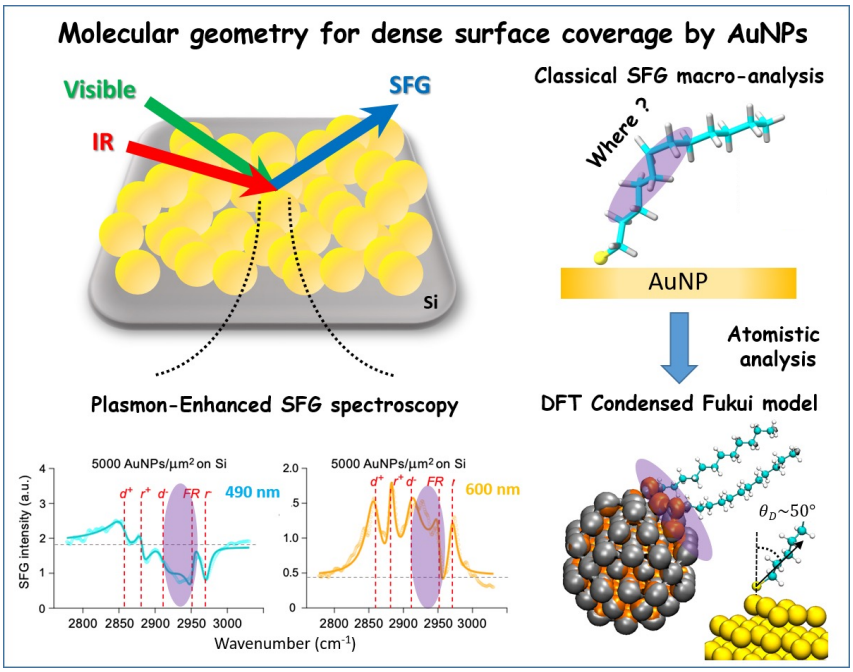

Highlights

Addressing molecular geometry on dense gold nanoparticle substrates by two-colour sum-frequency generation spectroscopy combined with DFT calculations

Grégory Barbillon, Christophe Humbert, Carine Clavaguéra, Audrey Gayral, Lidia Martínez, Yves Huttel, José Miguel García-Martín

- Combination of experimental (2C-SFG) and theoretical (DFT) steps in 3D space revealed local geometry of DDT molecule.

- Determination of local molecular geometry with DFT calculations (condensed Fukui analysis, computed IR/Raman spectra and DORI analysis).

- Precise location of molecular gauche defects in long interacting alkane chains for DDT molecules.

Addressing molecular geometry on dense gold nanoparticle substrates by two-colour sum-frequency generation spectroscopy combined with DFT calculations

Grégory Barbillon[a,b], Christophe Humbert[c], Carine Clavaguéra[c], Audrey Gayral[c], Lidia Martínez[d], Yves Huttel[d], José Miguel García-Martín[e]

[a]*EPF-Engineering School, 55 Avenue du Président Wilson, 94230 Cachan, France.*
[b]*Laboratoire Interfaces et Systèmes Electrochimiques, Sorbonne Université, CNRS, UMR 8235, LISE, 75005 Paris, France.*
[c]*Institut de Chimie Physique, Université Paris-Saclay, CNRS, UMR8000, 91405 Orsay, France.*
[d]*Instituto de Ciencia de Materiales de Madrid (ICCM), CSIC (CEI UAM+CSIC), Sor Juana Inés de la Cruz 3, 28049 Cantoblanco, Madrid, Spain.*
[e]*Instituto de Micro y Nanotecnología (IMN-CNM), CSIC (CEI UAM+CSIC), Isaac Newton 8, 28760 Tres Cantos, Madrid, Spain.*

Abstract

The geometrical conformations of dodecanethiol (DDT) molecules grafted on small gold nanoparticles (AuNPs, 7.5 nm diameter) deposited with various densities on a substrate were detected by two-color sum-frequency generation (SFG) spectroscopy. The high level of gauche defects indicates a L-shape structure of the alkane chains calculated classically through the amplitude ratios of the resonant modes of vibration for CH_2 methylene and CH_3 methyl groups (d^+/r^+ and d^-/r^-). Our amplitude ratios are higher than those found in the existing literature, and such effect can be ascribed to the combined action of several phenomena highlighting the geometrical molecular complexity on metal spheres: i) the matching of the visible wavelength of excitation with the plasmonic resonance of either isolated AuNPs (490 nm) or AuNPs multimers (600 nm), and ii) the local field enhancement. Additionally, we apply Density Functional Theory calculations on gold clusters functionalized by DDT molecules in interaction in a 3D space. By comparison with SFG results, we evidence through condensed Fukui analysis and computed IR/Raman spectra that the CH_2 methylene gauche defect in the alkane chain is present in the first one located beyond the sulfur atom giving precise insight on molecular geometry.

Keywords: Sum Frequency Generation, Plasmonics, Gold Nanoparticles, Dodecanethiol, Density Functional Theory

1. Introduction

Over the last ten years, the interest for the gold nanoparticles (AuNPs) has significantly increased due to their good chemical stability and their localized surface plasmon resonance (LSPR) adjustable in the spectral range from visible to near-infrared wavelengths [1, 2, 3]. AuNPs are largely employed in Raman spectroscopy such as surface-enhanced Raman scattering (SERS) in order to enhance the Raman signal of molecular vibration modes (ω_{mol}) thanks to the excitation of their plasmonic resonance [4, 5, 6, 7, 8, 9]. Similarly, AuNPs can be also used in surface non-linear optical spectroscopy based on sum-frequency generation (SFG: $\omega_{SFG} = \omega_{IR} + \omega_{Vis}$) processes [10] through the combination of infrared (ω_{IR}) and visible (ω_{Vis}) laser beams for enhancing the SFG signal of molecular vibration modes ($\omega_{mol} = \omega_{IR}$) by complementary and specific exploitation of their plasmonic resonance [11, 12, 13]. SFG spectroscopy is a vibrational probe permitting to investigate the molecular conformation [14, 15] of chemical or biological species [16, 17, 18, 19], and to study their dynamics over a surface or at an interface between two media differing by their nature or their physical phase [20, 21, 22, 23, 24]. SFG spectroscopy is surface sensitive within the electric dipole approximation because the molecules probed at the interface should be simultaneously IR (transition dipole moment) and Raman (Raman polarizability) active, a situation occurring when the electronic centrosymmetric character (geometrical parameter) of the system is broken, i.e. at interfaces or inside nonlinear crystals. SFG spectroscopy is therefore intrinsically more sensitive to conformational changes of molecules [25, 26, 27] than methods such as Raman spectroscopy and Fourier transform infrared one. Moreover, the SFG technique allows detecting a low percent of a monolayer of molecules on the surface of nanoparticles [28, 29, 31, 32]. Various research groups have studied the surfaces of metallic nanoparticles and nanoarrays or different nanostructured surfaces [37, 36, 33, 34, 35, 38]. In these different studies, the size of nanoparticles or nanostructures was comprised between 10 nm and 150 nm. For the most recent studies, Linke et al. have demonstrated plasmonic effects of AuNPs on the SFG spectrum of the molecule of 4-nitrothiophenol with AuNP sizes of 50 nm and 80 nm [33]. In addition, Tan et al. have reported effects of local field on SFG signals of poly(methyl methacrylate) (PMMA) films thanks to AuNPs of 40 nm [34]. In another study, Ma et al. have shown that chiral AuNPs allowed to generate sum-frequency electronic resonances, where the size of these chiral AuNPs was around 100 nm [35]. Furthermore, Dalstein et al. have reported on the role of hotspots in SFG spectroscopy enhanced by plasmon by using AuNPs of 13–14 nm deposited on silicon substrate [36]. They

Email address: gregory.barbillon@epf.fr (Grégory Barbillon)

also investigated in another work the effect of AuNPs (13–14 nm) on the SFG signal of methylene (CH_2) and methyl (CH_3) groups of the dodecanethiol (DDT) molecule, when deposited on a functionalized silicon substrate [37]. Furthermore, a couple of groups have used nanostructures below 10 nm for different studies employing SFG vibrational spectroscopy, such as the structure sensitivity in platinum (Pt) nanoparticles (0.9–6.7 nm) [39], the CO adsorption on palladium (Pd) nanoparticles (3–6 nm) [40], and the probing of the geometry of Pd nanoparticles (clusters from 4 atoms to 500 atoms) [41]. However, for investigations concerning the enhancement of the SFG signal or the analysis of the conformation of molecules on AuNPs whose size reaches those of molecules adsorbed on their surface, these latter were little addressed [28, 29] although advanced computational methods already developed for Self-Assembled Monolayers (SAM) of molecules grafted on flat surfaces, based on geometrical [42, 43, 44] or Density Functional Theory (DFT) calculations [45], could give access to the abundant and rich scientific information unveiled by SFG spectroscopy.

In this work, we report an investigation of the conformation of DDT molecules on the surface of small AuNPs (diameter of 7.5 nm) deposited on silicon (Si) substrate or 50 nm-thick Au film deposited on Si substrate for different densities of AuNPs by two-color sum-frequency generation spectroscopy (2C-SFG). We use two visible wavelengths in SFG experiments, the first one at 490 nm located at the level of the main d–s interband electronic transition of gold [32, 46, 47, 48] but also close to the LSPR of our small AuNPs (around 500 nm) deposited on silicon substrate, and the second one at 600 nm corresponding to a plasmonic resonance of multimers present in the samples, in comparison to the existing literature [28, 29, 36], where relevant works only used a fixed wavelength of excitation equal to 800 nm located far from AuNPs LSPR [28, 29]. Besides, as it is not possible to consider our samples as constituted of DDT-SAM adsorbed onto a flat 2D surface because of the 3D geometry of our AuNPs, we go beyond the above established molecular geometry calculations employed to deduce the orientation of molecules used here by implementing an appropriate DFT computational method at the atomic level on reference systems based on AuNPs clusters where two DDT molecules are grafted. Since we present a model of AuNP interacting with one or two DDT-S molecules, the well-established staple motif involving a large number of ligands has not been taken into account for the calculations [30]. DFT calculations shows that the interaction of two DDT molecules on curved metal surfaces already induces the presence of a L-shape structure whose gauche defect is originated in the first CH_2 of the alkane chain located near the gold atoms through condensed Fukui analysis performed on DDT-functionalized gold clusters, leading to deduce the local molecular tilt angles. We show that combining these atomistic theoretical and macroscopic experimental complementary methods gives precise reliable information on the local molecular geometry.

2. Experimental and Computational Methods

2.1. Sample Fabrication

AuNPs were grown using a standard gas aggregation source (GAS) from Oxford Applied Research Ltd. equipped with a 2 inches diameter full face erosion (FFE) magnetron from Nano4Energy SL. The FFE magnetron that is filled with rotating magnets generates a much more uniform erosion of the sputtering target and extends its lifetime [49] while it also eliminates the well-known fluctuations of the NP generation caused by the racetrack formation in standard magnetrons [50, 51]. The magnetron was positioned at an aggregation distance of 100 mm from exit slit and a stable argon flux of 80 sccm gas was injected through a mass flow controller. The FFE magnetron was operated at a power of 90 W and a current of 0.21 A, and the NPs were collected in an ultra-high vacuum chamber (base pressure in the high 10^{-10} mbar) connected to the GAS on the desired substrate (Si wafer or Si wafer with Au layer). When needed, the 50 nm thick Au film was deposited by standard magnetron sputtering using a magnetron source from AJA International Inc. with a circular Au target (3.8 cm diameter) and 19 cm distance between the Si substrate and the target. Argon was the sputter gas at a pressure of 1.5×10^{-3} mbar, and DC excitation at a 100 W constant power was used.

2.2. AFM Measurements

AFM measurements were performed using the Cervantes AFM System equipped with the Dulcinea electronics from Nanotec Electronica S.L. and acquired in tapping mode using tips with a nominal force constant of 2.8 $N.m^{-1}$ and a tip radius $<$ 10 nm. All AFM measurements were analysed using WSxM software [52].

2.3. Reflectance Measurements

To record reflectance spectra, a Cary-5000 spectrometer (Agilent) was used in a reflection configuration with an incidence angle of 7° with the surface normal due to the fact that the silicon substrate is a reflecting material in the spectral range of visible. The reflectance was determined by employing the following expression Reflectance = $\log_{10}(R_0/R)$ where R_0 and R are the reflectivity measurements of the silicon substrate without AuNPs (serving as reference) and the AuNPs on silicon substrate, respectively.

2.4. Dodecanethiol Deposition

Prior molecular functionalization, the samples were illuminated by UV light in order to remove any possible organic contamination of the AuNPs. To graft chemically the dodecanethiol (DDT, $CH_3(CH_2)_{11}$-SH, Sigma Aldrich) molecules on the surface of AuNPs, the samples were dipped in a 10^{-3} M solution of DDT in absolute ethanol (Sigma Aldrich) for 24 hours. Then, the samples have been carefully rinsed within three baths of absolute ethanol to remove possible DDT multilayers and dried with nitrogen flow before direct analysis by SFG spectroscopy. It is worth noting that in our case, it is not possible to have a well-ordered self-assembly process of

the molecules as on flat (poly)crystalline surfaces because of the surface curvature of AuNPs in a 3D space. We obtained therefore samples with DDT-adsorbed monolayers but no well-ordered SAM as defined in reference literature on organosuflur compounds [53, 54].

2.5. Two-Color Sum-Frequency Generation Spectroscopy

SFG spectra are acquired owing to a homemade setup based on a pulsed IR laser source from Quantel-Laser (Nd:YAG, 1064 nm, 12 ps) coupled to an acousto-optic modulator (100 MHz micropulse repetition rate, 1.5 μs train, 25 Hz macropulse repetition rate) described elsewhere [32]. After an amplification stage, the laser source pumps two optical parametric oscillators (OPO). The infrared one is tunable over the 2800–3000 cm^{-1} spectral range, while the visible one is fixed at 490 and 600 nm for each sample, respectively. As sketched in Fig. 1 for vibrational SFG spectra, the tunable IR and the fixed visible laser beams are coherently mixed at the same point of the sample surface with 65° and 55° incidence angles with respect to the surface normal direction, respectively. The polarization scheme is *ppp* for the SFG, visible, and IR beams. The SFG beam is therefore collected by a photomultiplier after spatial and spectral filtering through a double-stage monochromator. SFG data are normalized by the IR and visible powers for each wavelength to compensate for potential laser sources power fluctuations. Furthermore, the frequency resolution of the infrared OPO is equal to 3 cm^{-1} (as indicated in Tables S1 and S2 of supplementary data). The experimental SFG spectra are fitted with the expressions (1), (2), and (3) whose parameters are presented in Tables S1 and S2 in supplementary material where the detailed fitting procedure is given in section II of the latter.

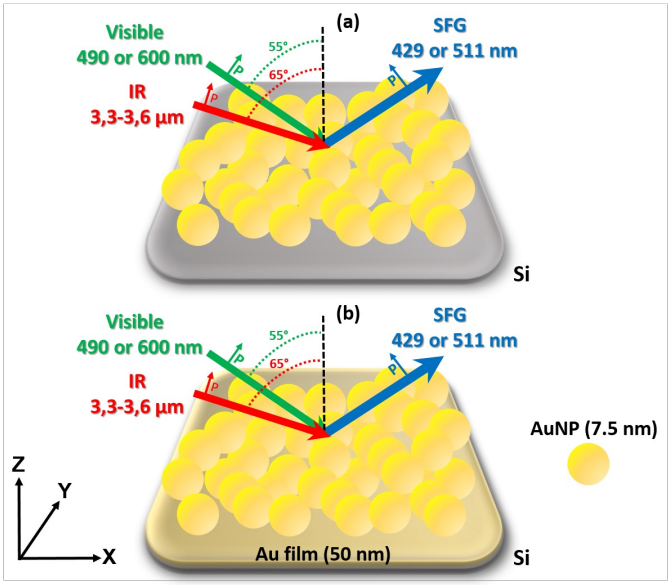

Figure 1: Scheme of the SFG experimental *ppp*-polarization scheme (*p*-polarized SFG, Vis, IR beams): (a) for AuNPs on Si substrate, and (b) for AuNPs on a gold film (50 nm) deposited on Si substrate.

2.6. DFT Calculations for Functionalized Gold Nanoparticles

DFT calculations have been carried out to optimize the structures and vibrational spectra of functionalized gold nanoparticles. The size of the system to be considered is then limited by the computational cost. Two models were chosen in the nanometer range, corresponding to clusters of 0.9 nm for Au_{38} and 1.4 nm for Au_{92}. One or two dodecanethiolate (DDT-S, $CH_3(CH_2)_{11}$-S) molecules adopting a linear shape were added close to the surface. Several starting points were tested for geometry optimization on corner and edges positions which have been previously proven to be more reactive than face positions [55]. The most energetically stable structures with a linear geometry of DDT are reported in Section IV of supplementary data (see Fig. S2). DFT calculations were done using the ORCA 5.0.3 software [56]. The geometry optimization calculations were performed using the PBE functional, the SDD quasi-relativistic pseudopotential (with 19 valence-electrons treated explicitly) and its associated basis set for gold atoms, and the def2-TZVP basis set for sulfur, carbon and hydrogen atoms. Dispersion corrections were added to the functional used in the D3 framework proposed by Grimme with the addition of the Beck–Johnson damping (D3BJ)[57]. The structures have been optimized without any geometrical constraints. For all the calculations, the 38-atom and 92-atom NPs (Au_{38}NP and Au_{92}NP) were considered in the singlet spin state. Numerical harmonic frequencies were calculated to ensure the structures corresponded to energy minima and to provide the IR spectral intensities. In order to compute the Raman intensities, the polarizabilities were computed at all displaced geometries. A scaling factor of 0.975, calibrated to match the CH_3 asymmetric modes, was used for all frequencies. The same level of theory was used for the Au_{92}NP of 1.4 nm in interaction with two DDT-S molecules to compute the displayed IR and Raman spectra in Fig. S2 of supplementary data. The nature of the interactions was investigated using the Multiwfn code by analyzing the electron density generated from ORCA [58]. The analyses of both covalent and non-covalent interactions were calculated based on the Density Overlap Regions Indicator (DORI)[59]. The reactivity of the AuNPs was analyzed by computing the Fukui function [60] to identify the electrophilic and nucleophilic sites.

3. RESULTS AND DISCUSSION

Firstly, AuNPs with 7.5 nm diameter were grown on a Si substrate by using the method described in the experimental section 2.1. Four samples were fabricated with different densities of AuNPs on the Si surface: 2000 AuNPs/μm^2, 5000 AuNPs/μm^2, 8000 AuNPs/μm^2, and for the last one, 8000 AuNPs/μm^2 on 50 nm-thick gold film on Si substrate. Then, these samples have been characterized with atomic force microscopy (AFM). Fig. 2 displays some representative AFM images as well as the histogram of the AuNPs size with mean diameter of 7.5 nm obtained from AFM pictures. Furthermore, the densities of AuNPs given previously correspond approximately to nanoparticle coverages of 11, 28 and 45% of a gold

nanoparticle monolayer, respectively. The coverage of AuNPs seems apparently larger in the AFM pictures due to the convolution between the shape of the AFM tip and the AuNPs [61, 62].

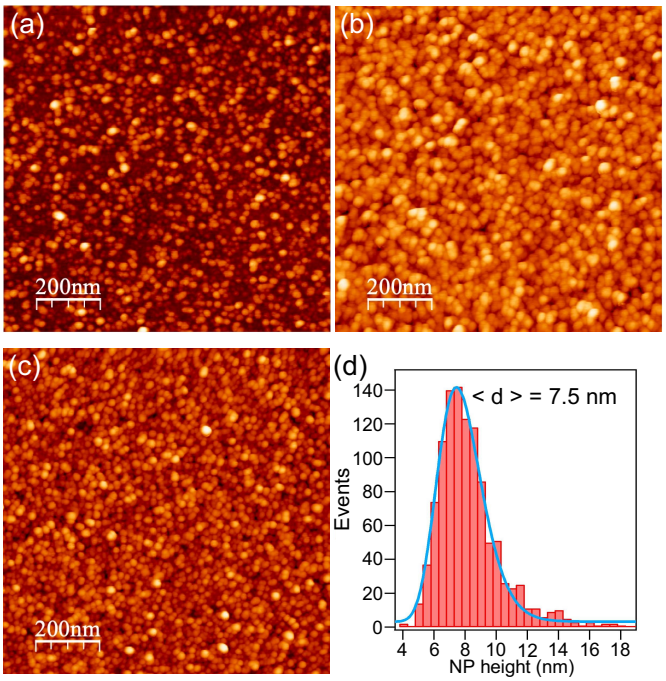

Figure 2: AFM pictures of AuNPs deposited on Si substrate for a density of (a) 2000 AuNPs/μm^2, (b) 8000 AuNPs/μm^2, and (c) 8000 AuNPs/μm^2 on 50 nm-thick gold film on Si substrate. (d) Histogram of the AuNPs size with mean diameter of 7.5 nm obtained from AFM pictures.

Next, the samples have been optically characterized by using visible reflectance measurements. For each sample, reflectance measurements were recorded with an incidence angle close to the normal to the surface. On each of these samples, a negative inflection was observed at a wavelength of 600 nm corresponding to a plasmonic resonance of multimers present in these latter (see Fig. 3). For the lowest density (see Fig. 3a), this inflection at 600 nm is clearly distinguished due to a significant presence of resonant hotspots at 600 nm while for the other densities (see Figs. 3 b,c,d), this inflection becomes less pronounced due to their "masking" by a larger presence of other plasmonic hotspots resonant at higher wavelengths. This inflection ("peak") is negative on reflectance spectra due to the presence of silicon and the incidence angle close to the normal upon reflectance measurements [32, 63, 64]. On each reflectance spectrum from Fig. 3, the two visible wavelengths selected for SFG measurements have been indicated. The first visible wavelength at 490 nm is located at the level of the d–s interband electronic transition of gold and close to the LSPR of AuNPs (around 500 nm, not discriminated in reflectance spectra of 4 samples due to the wide d–s electronic fingerprint). The second one was chosen at 600 nm for corresponding to the plasmonic resonance of multimers (collective surface plasmon resonance or CSPR) present in the samples. Afterwards, AuNPs were functionalized with DDT molecules according to the protocol described in the experimental section 2.4, where the effective surface of one AuNP exposed to DDT molecules is estimated to be 161 nm^2 (see Part V in supplementary data for details). Then, the number of DDT molecules grafted on gold nanoparticles was estimated, and we found 1.2 $\times$ 10^5, 3.1 $\times$ 10^5, 4.9 $\times$ 10^5 DDT molecules on the systems of 2000, 5000 and 8000 AuNPs/μm^2, respectively.

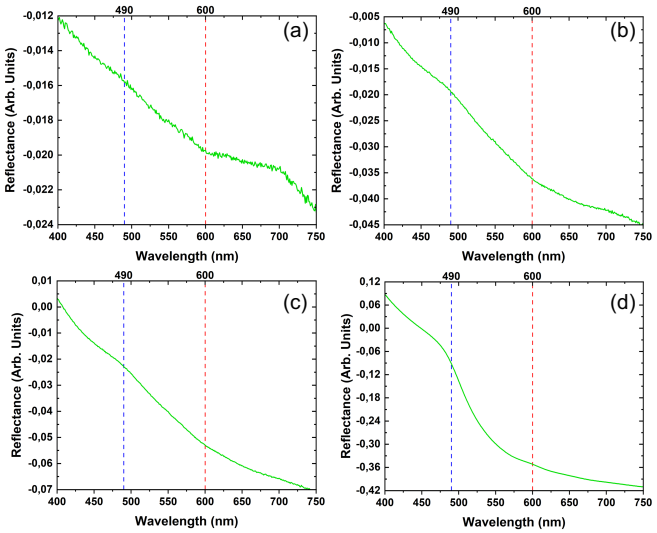

Figure 3: Reflectance spectra of AuNPs deposited on Si substrate for a density of (a) 2000 AuNPs/μm^2, (b) 5000 AuNPs/μm^2, (c) 8000 AuNPs/μm^2, and (d) 8000 AuNPs/μm^2 on gold film (50 nm thickness). The blue and red dashed lines correspond to the two visible wavelengths chosen for SFG measurements.

Following the functionalization, the SFG signal of DDT was measured on all samples by using the home-made 2C-SFG spectroscopy setup in the ppp-configuration (p-polarized SFG, Vis, IR beams; see Fig. 1) in order to probe methyl/methylene (CH_3/CH_2) stretching vibration modes in the 3.3–3.6 μm infrared spectral range, as detailed in the experimental section 2.5. The experimental intensity of the SFG signal is proportional to the square of the effective second-order non-linear susceptibility and can be expressed as follows [12, 15, 34, 65]:

$$I(\omega_{SFG}) \propto |\chi^{(2)}_{eff}|^2 = |\chi^{(2)}_{eff,mol} + \chi^{(2)}_{eff,NR}|^2 \quad (1)$$

with

$$\chi^{(2)}_{eff,mol} = \sum_{n=1}^{5} \frac{a_n e^{i\varphi_n}}{\omega_{IR} - \omega_n + i\Gamma_n} \quad (2)$$

$$\chi^{(2)}_{eff,NR} = A_{NR} e^{i\Phi_{NR}} \quad (3)$$

where a_n, φ_n, ω_n and Γ_n correspond to the amplitude, phase, frequency and damping constant for each of the five vibrational modes of the probed molecule (here DDT), respectively. In addition, A_{NR} and Φ_{NR} correspond to the amplitude and the phase coming from the optical activity of gold (i.e the non-resonant contribution, here the d–s interband electronic transition), respectively. $\chi^{(2)}_{eff,mol}$ represents the sum over Lorenztian oscillators describing here the five DDT CH_n (with n = 2 or 3) vibration modes (see Tables S1 and S2 in supplementary data).

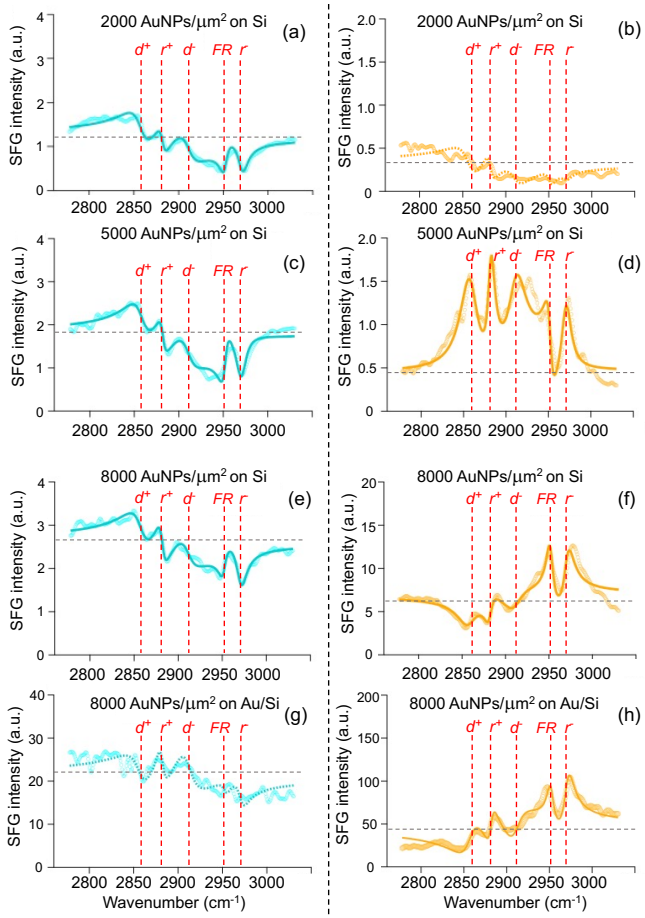

Figure 4: Experimental SFG spectra of DDT recorded at the two visible wavelengths of 490 nm (cyan circles) and 600 nm (yellow circles) in *ppp*-polarization scheme on the four samples with the following densities of AuNPs: (a) and (b) 2000 AuNPs/μm^2, (c) and (d) 5000 AuNPs/μm^2, (e) and (f) 8000 AuNPs/μm^2, and (g) and (h) 8000 AuNPs/μm^2 on 50 nm-thick gold film. The red dashed lines correspond to vibration modes d^+, d^-, r^+, r^-, and FR of DDT molecules. In each SFG spectrum, the cyan and gold lines, and the grey dashed line represent the fits of the SFG signal (using the expression (1)) and the non-resonant contribution of the SFG signal (background of gold), respectively. The cyan and gold dashed lines for Fig. 4b,g are guide to eye based on the fitting parameters obtained for Fig. 4a,h (see section II of supplementary data for explanation).

Fig. 4 displays the SFG vibrational fingerprint of DDT recorded for the two wavelengths (490 nm and 600 nm) on the samples with the four densities of AuNPs. On these SFG spectra, the five characteristic vibration modes observed corresponded to methyl (CH_3) and methylene (CH_2) groups [36, 37, 66, 67, 68]. For the methyl group, the vibration mode at 2882 cm^{-1} corresponds to the symmetric stretching mode (CH_3-SS, r^+), those at 2952 cm^{-1} and 2971 cm^{-1} are usually attributed to the Fermi resonance (CH_3-FR, FR) and the antisymmetric stretching mode (CH_3-AS, r^-), respectively. For the methylene group, the vibration mode at 2858 cm^{-1} corresponds to the symmetric stretching mode of the CH_2 group (CH_2-SS, d^+), that at 2911 cm^{-1} is attributed to the antisymmetric stretching mode (CH_2-AS, d^-). The experimental SFG spectra were fitted by using the expression (1). Strong SFG backgrounds corresponding to the d–s interband electronic transition of gold were observed for each SFG spectrum at the visible wavelength of 490 nm (see Fig. 4 a,c,e,g). When the AuNPs density increases so does this SFG signal background (and also with the addition of a gold layer under the AuNPs for the last sample of Fig. 4g. In this case, one magnitude order of SFG background is gained but to the detriment of the signal-to-noise ratio of the vibrational fingerprint, difficult to distinguish in these conditions, but perfectly distinguishable for the 600 nm visible wavelength in Fig. 4h). This is naturally related to the presence of more and more AuNPs in the probed zone (and also with the addition of the gold underlayer in the last sample). Moreover, clearly weaker SFG backgrounds of gold were also observed for each SFG spectrum at the visible wavelength of 600 nm (see Fig. 4b,d,f,h) due to the energy mismatch of the main d–s interband electronic transition of gold with the excitation visible wavelength of 600 nm. It should be noted that in Fig. 4b with the lowest AuNPs density, the vibrational fingerprint is hardly distinguishable due to a weak vibrational fingerprint signal-to-noise ratio. But the DDT vibration does appear clearly in Fig. 4a for the visible wavelength of 490 nm. In other words, playing with the visible light allows to detect the DDT vibration modes on each of the four samples. Nevertheless, the same increasing trend of the SFG signal background for both 490 nm and 600 nm visible excitation wavelengths was observed for increasing AuNPs densities, but also when the gold underlayer was added in the last sample (see Fig. 4 g,h). At the visible wavelength of 490 nm, the SFG intensities of the vibration modes are dip-shaped due to the presence of a strong non-resonant SFG background of gold interfering with Lorentzian-shaped SFG peaks. On contrary, at the visible wavelength of 600 nm, the SFG intensities of resonant modes of vibration are peak-shaped or Fano-like shaped due to the lower non-resonant SFG background of gold, thus interfering differently with Lorentzian-shaped peaks. These SFG spectral lineshapes were fitted following the detailed procedure based on Equations (1–3) given in section II of the supplementary material. Usually, it is common and sufficient to fix the phases of the vibration modes to zero (SAM films, very low density of AuNPs). In our case, it was not possible to keep this constraint to have convergence of the model with the experimental data. The best fits were obtained by letting them varying it freely. The best sets of fitting parameters, coherent in amplitudes, frequencies and damping constants for both wavelength are given in Tables S1 and S2 (see supplementary data). To justify the fact that the vibrational phases are let free, we considered that in our case, we have a very high density of AuNPs with respect to past literature. It induces the presence of numerous hotspots between close AuNPs having a considerable influence on the dipole transition moments μ_k and the Raman polarizabilities α_{ij} of the DDT molecules nonlinear 2^{nd} order polarizability (β_{ijk}) because of the intense local electromagnetic fields. Indeed, we work at excitation wavelengths in resonance with: (i) LSPR at 490 nm, in interference with the broad maximum of the d–s interband electronic contribution of gold; (ii) CSPR at 600 nm with a minimum of the d–s interband electronic contribution. In this case, it means that the DDT molecules are under-

Table 1: Comparison of amplitude ratios d^+/r^+ and d^-/r^- of the SFG signal versus the visible wavelength of excitation (λ_{Vis}) used in SFG experiments (ppp-polarization scheme) and the density of AuNPs (size of 7.5 nm; 8000* = 8000 AuNPs/μm^2 on the 50 nm-thick gold layer).

Density (AuNPs/μm^2)	λ_{Vis} (nm)	d^+/r^+	d^-/r^-
2000	490	1.21	0.82
5000	490	0.99	0.64
8000	490	0.87	0.68
8000*	490	–	–
2000	600	–	–
5000	600	1.05	0.28
8000	600	0.96	0.46
8000*	600	1.17	0.76

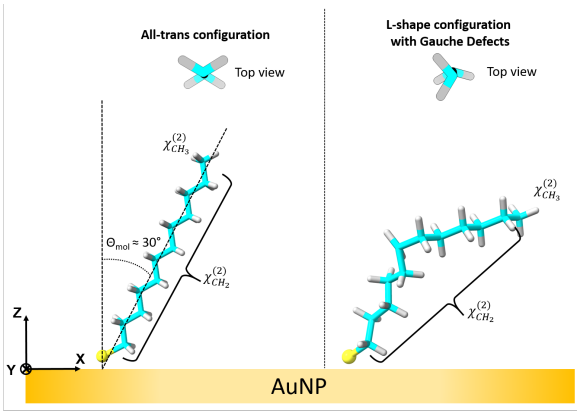

Figure 5: Principle schemes of the all-trans configuration and the L-shape configuration with gauche defects for DDT molecule on gold, and the description of the susceptibilities of resonant modes of dodecanethiol ($\chi^{(2)}_{CH_3}$, $\chi^{(2)}_{CH_2}$). Θ_{mol} represents the tilt angle of the DDT molecule in its all-trans configuration.

going strong energy transfers from the AuNPs plasmons, affecting μ_k and α_{ij}. Besides, due to the curvature effects of our small AuNPs in close contact, we also detect by SFG, thanks to plasmonic effects, CH_2 vibration modes at different specific locations in the alkane chains of a same molecule or in neighgbouring molecules, not well aligned and organized as in SAM (for a general in-depth treatment of the phase parameter in SAM films in nonlinear optical spectroscopy, see this reference [44]). DFT calculations presented further in our work will evidence this latter point. From these supplementary physical considerations, it is therefore reasonable to let the vibrational phases varying freely to obtain the best fitting convergence with the experimental data. Then, for determining experimentally the conformation of DDT molecules as sketched in Fig. 5, we calculated the amplitude ratios d^+/r^+ and d^-/r^- of the SFG signal for each density of AuNPs and the two excitation visible wavelengths (at 490 nm and 600 nm; see Table 1, and also the supplementary data for the formulas used for all these ratios).

By calculating the two amplitude ratios d^+/r^+ and d^-/r^-, we observe the presence of gauche defects in the DDT alkane chain, thus indicating a L-shape configuration for DDT molecules. Indeed, the emergence of the CH_2 stretching vibration modes in the SFG spectra confirms the presence of gauche defects and a L-shape configuration of the DDT alkane chain [26, 28, 29, 66, 69, 70] (see Fig. 5). Indeed, for well-ordered SAMs grafted on plane surface of gold (i.e alkyl chains are mainly aligned in the all-trans conformation), CH_2 vibration modes intensities are inferior to 10% of the CH_3 ones [28, 66, 71]. Besides, the tilt angle Θ_{mol} of the DDT alkane chain is between 27°–34° in its all-trans configuration, as reported in the literature [72, 73, 74, 75] (Θ_{mol} is the angle between the molecular axis of the alkane chain and the normal to the surface, see Fig. 5). Here, a Θ_{mol} value of 30° was adopted for the tilt angle of the DDT molecule [76].

In details, from the SFG spectra depicted in Fig. 4, we extracted and calculated the two amplitude ratios d^+/r^+ and d^-/r^-. For d^+/r^+, this ratio varied between 0.87 and 1.21, and between 0.96 and 1.17 for the excitation visible wavelengths at 490 nm and 600 nm, respectively. For d^-/r^-, this ratio evolved between 0.64 and 0.82, and between 0.28 and 0.76, respectively (see Table 1). These two ratios clearly indicated that the DDT molecules geometrical conformation on AuNPs of 7.5 nm had a L-shape configuration induced by a high level of gauche defects (see Fig. 5). From experimental SFG spectra, it is difficult to determine the localization of gauche defects. Thus, we have chosen to use DFT calculations in order to have a more precise idea of where is located the gauche defect and extract more realistic tilt angles by this advanced modelling method. While the common amplitude and intensity ratios method used for experimental angular determination in SFG spectroscopy performed on flat surfaces gives a qualitative and quantitative analysis of the molecular geometry on such surfaces, it does not take into account the chemical interactions between DDT alkane chains, gold atomic organization and the surface curvature at the AuNP surface as encountered in our complex systems because the notion of geometrical reference is puzzled on AuNPs. In other words, what is the normal direction to the sphere surface for alkane chains grafted in a three-dimensional (3D) space? To address this complex issue and gain valuable and analytical insights based on exact theoretical calculations, we have to switch from our common and limited geometrical 2D vision to a 3D space by exploring more robust computational methods. In order to illustrate our point, we introduce here an all-atom DFT computational method (see Computational section II F for details) to extract structural, electronic and spectroscopic information from models of one or two DDT-S molecules grafted on AuNPs of two different sizes: 0.9 nm and 1.4 nm (labeled Au_{38}NP and Au_{92}NP, respectively) as sketched in Fig. 6. For all the calculations, the DDT-S molecules interact by the S atom on the most reactive sites of the AuNP, with a single gold atom or two adjacent gold atoms without changing the qualitative nature of the interaction. Depending on the starting structure of the geometry optimization, several orientations of the DDT-S molecule on the AuNP surface were obtained depending on whether it could wrap around the surface or remain in a quasi-linear form. Only the quasi-linear structure is described in the following discussion with a single DDT-S molecule to be consistent with the model with two DDT-S molecules.

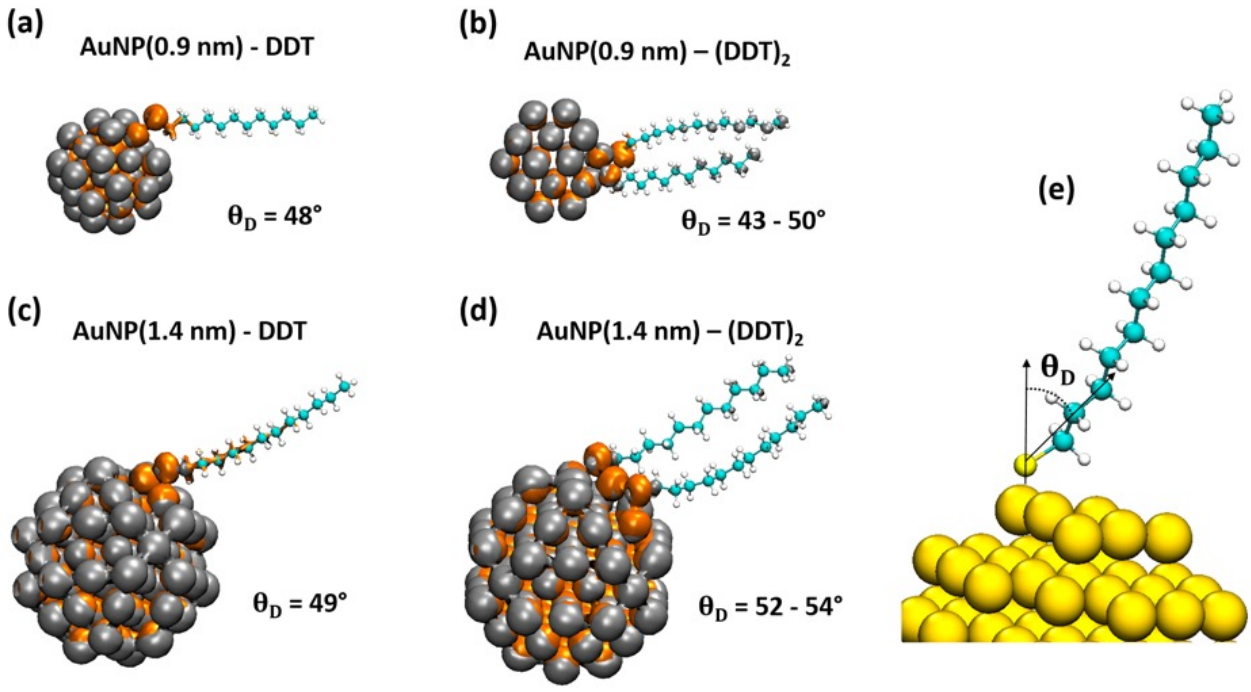

Figure 6: Condensed Fukui analysis of (a) AuNP(0.9 nm) - DDT; (b) AuNP(0.9 nm) - $(DDT)_2$; (c) AuNP(1.4 nm) - DDT; (d) AuNP(1.4 nm) - $(DDT)_2$. The grey and orange isosurfaces represent the electrophilic and nucleophilic sites, respectively. The angle θ_D in Figure (e) is the angle obtained from DFT analysis defined as the angle between the direction of the S and Au atom to which it is connected and the direction between the S and the 2^{nd} CH_2 group (from the AuNP).

The condensed Fukui functions are calculated to identify the nucleophilic and electrophilic regions predicting the local binding sites of the DDT-S at the AuNP surface (see Fig. 6). The electrophilic sites of the AuNPs are mostly located at the surface (grey color in Fig. 6). The nucleophilic sites remain mainly located at the sulfur atom, both around a few gold atoms and on the first CH_2 group close to the sulfur site (orange color in Fig. 6). In the cases of two DDT-S molecules, the S atoms interact with two adjacent gold atoms and the chains remain linear, weakly interacting with each other to stabilize the structure. DORI analysis is used to visualize the spatial organization of the intermolecular interactions (see Fig. S3 in supplemental data for DORI plots), with the green color clearly representing the dispersive interactions between the molecular chains. The spatial orientation of the DDT-molecules is also useful for deducing the tilt angle θ_D, which ranges between 48° and 54°, and increases with the size of the cluster (see Fig. 6 for θ_D individual values). Finally, the IR and Raman harmonic spectra are displayed in the 2800-3050 cm^{-1} spectral range in Fig. S2 and mode attributions are provided in Tables S3 and S4 (see Section IV of supplementary data). The DFT spectra are provided as a qualitative comparison with the experimental SFG data without attempting a very precise match. For both cluster sizes, this spectral range can be divided in different sub-ranges corresponding to the expected vibrational modes of the DDT chains, consistent with from SFG data fitting in Tables S1 and S2 (see supplementary data). For the IR spectrum of Au_{38}NP in interaction with two DDT, the 2960-2980 cm^{-1} band corresponds to the CH_3-AS (r^-) mode with a medium intensity, which was used to calibrate the computed data with the experimental frequency at 2971 cm^{-1}. The band at 2950 cm^{-1} corresponds to the CH_2-AS mode of the first CH_2 group after the sulfur atom (CH_2[1]-AS), in agreement with the experimental frequency at 2952 cm^{-1}. This group is in a different chemical environment, resulting in a frequency shift compared to the other CH_2 groups. It is worth noting here that, from DFT calculations (see Table S4 in supplementary data), this is a different attribution with respect to the CH_3-FR (FR) mode of our Table S1 (see supplementary material), often presumed in SFG history for this archetype reference molecule. In fact, we observe that this specific spectral range is broad and difficult to fit perfectly by equations (1-3) in Fig. 4 c,d with only one vibration mode. DFT calculations shows that the presence of CH_2[1]-AS vibration mode on AuNPs with a significant intensity can explain these spectral features. This is equally the location on the alkane chain where the gauche defects appear due to the surface curvature in 3D space, which affects differently the chemical bonding to gold atoms with respect to a crystalline flat surface in 2D space.

To complete this study, we compared these results of amplitude ratios d^+/r^+ and d^-/r^- with existing literature [29, 36] (see Table 2). This comparison was carried out by taking into account that the polarization scheme of the SFG experiments (here, ppp-polarization scheme) is the same. From Table 2, we

Table 2: Comparison of amplitude ratios d^+/r^+ and d^-/r^- of the SFG signal versus the excitation wavelength (λ_{exc}) used in SFG experiments (ppp-polarization scheme) and the size of AuNPs.

AuNP size	λ_{exc} (nm)	d^+/r^+	d^-/r^-	Ref.
7.5 nm	490	0.87 – 1.21	0.64 – 0.82	This Work
7.5 nm	600	0.96 – 1.17	0.28 – 0.76	This Work
1.8 nm	800	0.62	0.39	[29]
2.9 nm	800	0.4	0.17	[29]
7.4 nm	800	0.31	< 0.01	[29]
13.5 nm	488	< 0.01	< 0.01	[36]
13.5 nm	594	< 0.01	< 0.01	[36]

Table 3: Calculations of the enhancement factor (EF) as a function of the density of AuNPs (EF_{EM} = electromagnetic enhancement coming from the matching of a plasmon resonance with visible and SFG beams, and EF_{LF} = enhancement of the local field; 8000* = 8000 AuNPs/μm^2 on the 50 nm-thick gold layer; see supplementary material for more details of EF calculations).

Enhancement Factor	2000	5000	8000	8000*
EF (λ_{Vis} = 490 nm; λ_{SFG} = 429 nm)	4.69	6.17	6.71	6.91
EF (λ_{Vis} = 600 nm; λ_{SFG} = 511 nm)	31.71	72.49	73.12	208.44
EF_{LF} (λ_{Vis} = 490 nm; λ_{SFG} = 429 nm)	1.89	2.09	2.20	2.31
EF_{LF} (λ_{Vis} = 600 nm; λ_{SFG} = 511 nm)	3.80	5.39	5.31	7.61
EF_{EM} (λ_{Vis} = 490 nm; λ_{SFG} = 429 nm)	2.48	2.95	3.05	2.99
EF_{EM} (λ_{Vis} = 600 nm; λ_{SFG} = 511 nm)	8.34	13.45	13.77	27.39

noted that for similar or smaller sizes of AuNPs (diameters of 1.8 nm and 2.9 nm), our amplitude ratios d^+/r^+ and d^-/r^- were higher or similar than those presented in Bordenyuk et al work [29] due to the fact that they used an excitation wavelength of 800 nm far from a plasmon resonance, whereas we used two selective and discriminating visible wavelengths at 490 nm and 600 nm corresponding either to a plasmonic resonance of isolated AuNPs (LSPR) or multimers (CSPR, coupling between AuNPs), respectively. Moreover, this was also due to an effect of the local field. Indeed, enhancement factors (EFs) comprised between 4.69 and 208.44 were calculated with the following expression [34]:

$$EF \propto g_{SFG}^2 g_{Vis}^4 \tag{4}$$

where $g_{SFG}^2 g_{Vis}^2$ (named EF_{EM}) and g_{Vis}^2 (named EF_{LF}) correspond to the electromagnetic enhancement coming from the matching of a plasmon resonance with visible and SFG beams, and the enhancement of the local field [34], respectively (see Table 3 and supplementary material for the EF calculation). We observed higher EFs at the excitation wavelength of 600 nm than those at 490 nm due to the damping of the interband transition present at 490 nm. In addition, the enhancement of the local field (EF_{LF}), especially between the AuNPs and the substrate [77] (Si or Au film), varied from 1.89 to 7.61 coming from the interference between AuNPs and their images induced by the substrate [78] (Si or Au film). Besides, the enhancement factors (EF) calculated for our experiments are relatively weak due to the fact that the size of our AuNPs is small.

Furthermore, by comparing our results of these ratios with those of Dalstein et al [36] at similar excitation wavelengths, the values of our amplitude ratios were higher than theirs, which were around zero due to the fact that a better organization is obtained with their gold nanoparticles (13.5 nm) than with ours. Nevertheless, they observe the appearance of CH_2 vibration modes taken into account in their SFG fitting procedure as detailed in their supplementary material. This better organization is due to the formation of small SAMs (well-ordered) on their facets [36, 79, 80]. Indeed, on their AuNPs and also on planar gold, it is known that long chains of alkanethiols favor lateral interactions leading to a long-range molecular order [80].

4. CONCLUSION

Herein, we reported the geometrical conformation of DDT molecules on 7.5 nm diameter AuNPs as a function of their density on a Si substrate with or without an intermediate gold film (50 nm thick). We observed that DDT molecules had a conformation with a high level of gauche defects indicating a L-shape on these AuNPs, as directly deduced from SFG measurements at the two visible excitation wavelengths by calculating the amplitude ratios d^+/r^+ and d^-/r^-. The obtained values of these ratios were higher than those found in the existing literature, this fact can be highlighted thanks to the matching of the visible wavelength with plasmonic resonances of isolated AuNPs (LSPRs) and multimers, respectively. Additionally, this is accompanied by an enhancement of the local field. Furthermore, we observed that the enhancement factor increased when the density of gold nanoparticles increased and more largely at the excitation wavelength of 600 nm corresponding to the plasmonic resonance of multimers. Thus, the plasmonic enhancement of the SFG signal recorded with small AuNPs whose size is close to the molecule to be studied can allow the detection of multiple geometrical conformations on complex surfaces (e.g. AuNPs deposited with various densities on a substrate). Moreover, this plasmonic enhancement can provide a better understanding of the ultrafast dynamics nearby plasmonic systems, which can be applied to domains such as catalysis and photovoltaics enhanced by plasmons. Furthermore, it is difficult to determine the localization of gauche defects from experimental SFG spectra. Thus, we used a relevant DFT computational method based on two DDT molecules grafted on gold clusters of 0.9 et 1.4 nm size, showing that their interaction in a 3D space already induced gauche defects in the alkane chain but at the level of the first methylene group located just beyond the sulfur atom bounded to the gold atom as deduced from condensed Fukui analysis and computed IR and Raman spectra in the energy range of interest. To the best of our knowledge, this is the first time that DFT calculations are used to bridge the gap between the classical macro-analysis of SFG spectra exploring molecular geometry on 2D surfaces and a DFT Condensed atomistic Fukui analysis coupled to spectral simulations of relatively big 3D clusters from the computational point of view. The latter methods give a precise geometrical location of gauche defect in alkane chains for which orientation can also be deduced. Other molecules containing multiple functional groups like substituted aromatic molecules, which can feature a

variety of interactions, could be envisaged to extend this combined experimental and theoretical study. For a direct comparison with SFG experiments, molecular simulations would have to be applied on a larger size scale, including the simulation of SFG signals. Due to the very high computational costs of DFT simulations for such complex structures, new methodologies are currently being developed, but this is beyond the scope of this study. We hope this first combined experimental and theoretical step in 3D space for computing molecular geometry at the nanoscale in the framework of 2C-SFG spectroscopy will enlarge the nonlinear optics universe coupled to DFT methods.

CRediT authorship contribution statement

G. Barbillon: Conceptualization, Formal analysis, Investigation, Supervision, Validation, Visualization, Writing – original draft, Writing – review & editing. **C. Humbert:** Conceptualization, Formal analysis, Investigation, Resources, Supervision, Validation, Visualization, Writing – original draft, Writing – review & editing. **C. Clavaguéra:** Formal analysis, Investigation, Resources, Validation, Visualization, Writing – original draft, Writing – review & editing. **A. Gayral:** Investigation, Resources, Writing – review & editing. **L. Martínez:** Formal analysis, Investigation, Resources, Validation, Visualization, Writing – original draft, Writing – review & editing. **Y. Huttel:** Conceptualization, Formal analysis, Investigation, Resources, Supervision, Validation, Visualization, Writing – original draft, Writing – review & editing. **J.M. García-Martín:** Conceptualization, Formal analysis, Investigation, Supervision, Validation, Visualization, Writing – original draft, Writing – review & editing.

Declaration of competing interest

The authors declare that they have no known competing financial interests or personal relationships that could have appeared to influence the work reported in this paper.

Data availability

Data will be made available on request.

Acknowledgements

Yves Huttel, Lidia Martínez and José Miguel García-Martín acknowledge grant PID2021-126524NB-100 funded by MCIN/AEI/10.13039/501100011033 and by "ERDF A way of making Europe".

Appendix A. Supplementary data

The amplitude ratio (d^+/r^+ and d^-/r^-) calculations, the fitting procedure, the calculation of the enhancement factor (EF), the DFT harmonic IR/Raman spectra and corresponding tables of vibration mode frequencies, and the DORI analysis for the systems modeled in this work are provided in supplementary data. Supplementary material related to this article can be found online at `https://doi.org/10.1016/j.apsusc.2024.161817`.

References

[1] K. A. Willets, R. P. Van Duyne, Localized Surface Plasmon Resonance Spectroscopy and Sensing, Annu. Rev. Phys. Chem. 58 (2007) 267–297.
[2] S. Barbosa, A. Agrawal, L. Rodríguez-Lorenzo, I. Pastoriza-Santos, R. A. Alvarez-Puebla, A. Kornowski, H. Weller, L. M. Liz-Marzan, Tuning Size and Sensing Properties in Colloidal Gold Nanostars, Langmuir 26 (2010) 14943–14950.
[3] G. A. Vinnacombe-Willson, Y. Conti, A. Stefancu, P. S. Weiss, E. Cortés, L. Scarabelli, Direct Bottom-Up *In Situ* Growth: A Paradigm Shift for Studies in Wet-Chemical Synthesis of Gold Nanoparticles, Chem. Rev. 123 (2023) 8488–8529.
[4] N. L. Gruenke, M. F. Cardinal, M. O. McAnally, R. R. Frontiera, G. C. Schatz, R. P. Van Duyne, Ultrafast and nonlinear surface-enhanced Raman spectroscopy, Chem. Soc. Rev. 45 (2016) 2263–2290.
[5] A. B. Zrimsek, N. Chiang, M. Mattei, S. Zaleski, M. O. McAnally, C. T. Chapman, A. -I. Henry, G. C. Schatz, R. P. Van Duyne, Single-Molecule Chemistry with Surface- and Tip-Enhanced Raman Spectroscopy, Chem. Rev. 117 (2017) 7583–7613.
[6] J. Reguera, J. Langer, D. Jiménez de Aberasturi, L. M. Liz-Marzan, Anisotropic metal nanoparticles for surface enhanced Raman scattering, Chem. Soc. Rev. 46 (2017) 3866–3885.
[7] C. Zong, M. Xu, L. -J. Xu, T. Wei, X. Ma, X. -S. Zheng, R. Hu, B. Ren, Surface-Enhanced Raman Spectroscopy for Bioanalysis: Reliability and Challenges, Chem. Rev. 118 (2018) 4946–4980.
[8] G. Barbillon, Latest Advances in Metasurfaces for SERS and SEIRA Sensors as Well as Photocatalysis, Int. J. Mol. Sci. 23 (2022) 10592.
[9] G. Barbillon, C. Humbert, M. U. González, J. M. García-Martín, Gold Nanocolumnar Templates for Effective Chemical Sensing by Surface-Enhanced Raman Scattering, Nanomaterials 12 (2022) 4157.
[10] X. D. Zhu, H. Suhr, Y. R. Shen, Surface vibrational spectroscopy by infrared-visible sum frequency generation, Phys. Rev. B 35 (1987) 3047–3050.
[11] D. Lis, Y. Caudano, M. Henry, S. Demoustier-Champagne, E. Ferain, F. Cecchet, Selective Plasmonic Platforms Based on Nanopillars to Enhance Vibrational Sum-Frequency Generation Spectroscopy, Adv. Optical Mater. 1 (2013) 244–255.
[12] C. Humbert, T. Noblet, L. Dalstein, B. Busson, G. Barbillon, Sum-Frequency Generation Spectroscopy of Plasmonic Nanomaterials: A Review, Materials 12 (2019) 836.
[13] M. Gao, Y. He, Y. Chen, T. -M. Shih, W. Yang, H. Chen, Z. Yang, Z. Wang, Enhanced sum frequency generation for ultrasensitive characterization of plasmonic modes, Nanophotonics 9 (2020) 815–822.
[14] P. Guyot-Sionnest, J. H. Hunt, Y. R. Shen, Sum-frequency vibrational spectroscopy of a Langmuir film: Study of molecular orientation of a two-dimensional system, Phys. Rev. Lett. 59 (1987) 1597–1600.
[15] X. Zhuang, P. B. Miranda, D. Kim, Y. R. Shen, Mapping molecular orientation and conformation at interfaces by surface nonlinear optics, Phys. Rev. B 59 (1999) 12632–12640.
[16] B. Ding, A. Panahi, J. -J. Ho, J. E. Laaser, C. L. Brooks, III, M. T. Zanni, Z. Chen, Probing Site-Specific Structural Information of Peptides at Model Membrane Interface In Situ, J. Am. Chem. Soc. 137 (2015) 10190–10198.
[17] X. Han, C. Leng, Q. Shao, S. Jiang, Z. Chen, Absolute Orientations of Water Molecules at Zwitterionic Polymer Interfaces and Interfacial Dynamics after Salt Exposure, Langmuir 35 (2019) 1327–1334.
[18] C. Zhang, G. A. Parada, X. Zhao, Z. Chen, Probing Surface Hydration and Molecular Structure of Zwitterionic and Polyacrylamide Hydrogels, Langmuir 35 (2019) 13292–13300.
[19] T. Lin, W. Guo, R. Guo, Z. Chen, Probing Biological Molecule Orientation and Polymer Surface Structure at the Polymer/Solution Interface In Situ, Langmuir 36 (2020) 7681–7690.
[20] Z. Zhang, L. Piatkowski, H. J. Bakker, M. Bonn, Ultrafast vibrational energy transfer at the water/air interface revealed by two-dimensional surface vibrational spectroscopy, Nat. Chem. 3 (2011) 888–893.

[21] P. C. Singh, K. Inoue, S. Nihonyanagi, S. Yamaguchi, T. Tahara, Femtosecond Hydrogen Bond Dynamics of Bulk-like and Bound Water at Positively and Negatively Charged Lipid Interfaces Revealed by 2D HD-VSFG Spectroscopy, Angew. Chem., Int. Ed. 55 (2016) 10621–10625.

[22] S. Nihonyanagi, S. Yamaguchi, T. Tahara, Ultrafast Dynamics at Water Interfaces Studied by Vibrational Sum Frequency Generation Spectroscopy, Chem. Rev. 117 (2017) 10665–10693.

[23] J. C. Flanagan, M. L. Valentine, C. R. Baiz, Ultrafast Dynamics at Lipid–Water Interfaces, Acc. Chem. Res. 53 (2020) 1860–1868.

[24] S. Hosseinpour, S. J. Roeters, M. Bonn, W. Peukert, S. Woutersen, T. Weidner, Structure and Dynamics of Interfacial Peptides and Proteins from Vibrational Sum-Frequency Generation Spectroscopy, Chem. Rev. 120 (2020) 3420–3465.

[25] R. Lu, W. Gan, B. -H. Wu, Z. Zhang, Y. Guo, H. -F. Wang, C–H Stretching Vibrations of Methyl, Methylene and Methine Groups at the Vapor/Alcohol (n = 1–8) Interfaces, J. Phys. Chem. B 109 (2005) 14118–14129.

[26] A. N. Bordenyuk, H. Jayathilake, A. V. Benderskii, Coherent Vibrational Quantum Beats as a Probe of Langmuir–Blodgett Monolayers, J. Phys. Chem. B 109 (2005) 15941–15949.

[27] C. S. Tian, Y. R. Shen, Recent progress on sum-frequency spectroscopy, Surf. Sci. Rep. 69 (2014) 105–131.

[28] C. Weeraman, A. K. Yatawara, A. N. Bordenyuk, A. V. Benderskii, Effect of Nanoscale Geometry on Molecular Conformation: Vibrational Sum-Frequency Generation of Alkanethiols on Gold Nanoparticles, J. Am. Chem. Soc. 128 (2006) 14244–14245.

[29] A. N. Bordenyuk, C. Weeraman, A. K. Yatawara, H. D. Jayathilake, I. Stiopkin, Y. Liu, A. V. Benderskii, Vibrational Sum Frequency Generation Spectroscopy of Dodecanethiol on Metal Nanoparticles, J. Phys. Chem. C 111 (2007) 8925–8933.

[30] D. Lin, M. Zheng, W. W. Xu, Structural predictions of thiolate-protected gold nanoclusters via the redistribution of Au-S "staple" motifs on known cores, Phys. Chem. Chem. Phys. 22 (2020) 16624–16629.

[31] O. Pluchery, C. Humbert, M. Valamanesh, E. Lacaze, B. Busson, Enhanced detection of thiophenol adsorbed on gold nanoparticles by SFG and DFG nonlinear optical spectroscopy, Phys. Chem. Chem. Phys. 11 (2009) 7729–7737.

[32] C. Humbert, O. Pluchery, E. Lacaze, A. Tadjeddine, B. Busson, Optical spectroscopy of functionalized gold nanoparticles assemblies as a function of the surface coverage, Gold Bull. 46 (2013) 299–309.

[33] M. Linke, M. Hille, M. Lackner, L. Schumacher, S. Schlückler, E. Hasselbrink, Plasmonic Effects of Au Nanoparticles on the Vibrational Sum Frequency Spectrum of 4-Nitrothiophenol, J. Phys. Chem. C 123 (2019) 24234–24242.

[34] J. Tan, Q. Pei, L. Zhang, S. Ye, Evidence for a Local Field Effect in Surface Plasmon-Enhanced Sum Frequency Generation Vibrational Spectra, Langmuir 38 (2022) 6099–6105.

[35] R. Ma, T. W. Golbek, Y. Shi, T. Weidner, D. Sutherland, Chiral Sum Frequency Generation by Chiral Gold Nanoparticles Amplifies Weak Sum Frequency Signals and Enables Monitoring of Enantioselective Reactions, ACS Appl. Nano Mater. 6 (2023) 16161–16167.

[36] L. Dalstein, C. Humbert, M. Ben Haddada, S. Boujday, G. Barbillon, B. Busson, The Prevailing Role of Hotspots in Plasmon-Enhanced Sum-Frequency Generation Spectroscopy, J. Phys. Chem. Lett. 10 (2019) 7706–7711.

[37] L. Dalstein, M. Ben Haddada, G. Barbillon, C. Humbert, A. Tadjeddine, S. Boujday, B. Busson, Revealing the Interplay between Adsorbed Molecular Layers and Gold Nanoparticles by Linear and Nonlinear Optical Properties, J. Phys. Chem. C 119 (2015) 17146–17155.

[38] G. Barbillon, T. Noblet, B. Busson, A. Tadjeddine, C. Humbert, Localised detection of thiophenol with gold nanotriangles highly structured as honeycombs by nonlinear sum frequency generation spectroscopy, J. Mater. Sci. 53 (2018) 4554–4562.

[39] W. D. Michalak, J. M. Krier, K. Komvopoulos, G. A. Somorjai, Structure Sensitivity in Pt Nanoparticle Catalysts for Hydrogenation of 1,3-Butadiene: *In Situ* Study of Reaction Intermediates Using SFG Vibrational Spectroscopy, J. Phys. Chem. C 117 (2013) 1809–1817.

[40] A. Ouvrard, A. Ghalgaoui, C. Michel, C. Barth, J. Wang, S. Carrez, W. Zheng, C. R. Henry, B. Bourguignon, Chemisorption on Ultrathin MgO-Supported Palladium Nanoparticles, J. Phys. Chem. C 121 (2017) 5551–5564.

[41] N. Alyabyeva, A. Ouvrard, A. M. Zakaria, B. Bourguignon, Probing Nanoparticle Geometry down to Subnanometer Size: The Benefits of Vibrational Spectroscopy, J. Phys. Chem. Lett. 10 (2019) 624–629.

[42] C. Hirose, N. Akamatsu, K. Domen, Formulas for the analysis of surface sum-frequency generation spectrum by CH stretching modes of methyl and methylene groups, J. Chem. Phys. 96 (1992) 997–1004.

[43] A. Yousefi, D. K. Hore, Using Structural Information to Fit Vibrational Sum Frequency Spectra, J. Phys. Chem. C 128 (2024) 7252–7265.

[44] A. P. Fellows, V. Balos, B. John, A. D. Duque, M. Wolf, M. Thämer, Obtaining extended insight into molecular systems by probing multiple pathways in second-order nonlinear spectroscopy, J. Chem. Phys. 159 (2023) 164201.

[45] F. Cecchet, D. Lis, Y. Caudano, A. A. Mani, A. Peremans, B. Champagne, J. Guthmuller, Density functional theory-based simulations of sum frequency generation spectra involving methyl stretching vibrations: effect of the molecular model on the deduced molecular orientation and comparison with an analytical approach, J. Phys. Cond. Matter 24 (2012) 124110.

[46] M. Bernardi, J. Mustafa, J. B. Neaton, S. G. Louie, Theory and computation of hot carriers generated by surface plasmon polaritons in noble metals, Nat. Commun. 6 (2015) 7044.

[47] J. Zhao, S. C. Nguyen, R. Ye, B. Ye, H. Weller, G. A. Somorjai, A. P. Alivisatos, F. D. Toste, A Comparison of Photocatalytic Activities of Gold Nanoparticles Following Plasmonic and Interband Excitation and a Strategy for Harnessing Interband Hot Carriers for Solution Phase Photocatalysis, ACS Cent. Sci. 3 (2017) 482–488.

[48] X. Zhang, C. Huang, M. Wang, P. Huang, X. He, Z. Wei, Transient localized surface plasmon induced by femtosecond interband excitation in gold nanoparticles, Sci. Rep. 8 (2018) 10499.

[49] Y. Huttel, L. Martínez, A. Mayoral, I. Fernández, Gas-phase synthesis of nanoparticles: present status and perspectives, MRS Commun. 8 (2018) 947–954.

[50] M. Ganeva, A. V. Pipa, R. Hippler, The influence of target erosion on the mass spectra of clusters formed in the planar DC magnetron sputtering source, Surf. Coat. Technol. 213 (2012) 41–47.

[51] A. Rai, A. Mutzke, G. Bandelow, R. Schneider, M. Ganeva, A. V. Pipa, R. Hippler, Operational limit of a planar DC magnetron cluster source due to target erosion, Nucl. Instrum. Methods Phys. Res., Sect. B 316 (2013) 6–12.

[52] I. Horcas, R. Fernández, J. M. Gómez-Rodríguez, J. Colchero, J. Gómez-Herrero, A. M. Baro, WSXM: a software for scanning probe microscopy and a tool for nanotechnology, Rev. Sci. Instrum. 78 (2007) 013705.

[53] G. E. Poirier, Characterization of Organosulfur Molecular Monolayers on Au(111) using Scanning Tunneling Microscopy, Chem. Rev. 97 (1997) 1117–1128.

[54] A. Ulman, Formation and Structure of Self-Assembled Monolayers, Chem. Rev. 96 (1996) 1533–1554.

[55] R. Tandiana, N. T. Van-Oanh, C. Clavaguéra, Interaction between organic molecules and a gold nanoparticle: a quantum chemical topological analysis, Theor. Chem. Acc. 140 (2021) 118.

[56] F. Neese, The ORCA program system, Wiley Interdiscip. Rev. Comput. Mol. Sci. 2 (2012) 73–78.

[57] S. Grimme, S. Ehrlich, L. Goerigk, Effect of the damping function in dispersion corrected density functional theory, J. Comput. Chem. 32 (2011) 1456–1465.

[58] T. Lu, F. Chen, Multiwfn: A multifunctional wavefunction analyzer, J. Comput. Chem. 33 (2011) 580–592.

[59] P. de Silva, C. Corminboeuf, Simultaneous Visualization of Covalent and Noncovalent Interactions Using Regions of Density Overlap, J. Chem. Theory Comput. 10 (2014) 3745–3756.

[60] R. G. Parr, W. Yang, Density functional approach to the frontier-electron theory of chemical reactivity, J. Am. Chem. Soc. 106 (1984) 4049–4050.

[61] J. Shen, D. Zhang, F. -H. Zhang, Y. Gan, AFM tip-sample convolution effects for cylinder protrusions, Appl. Surf. Sci. 422 (2017) 482–491.

[62] M. Ruano, M. Díaz, L. Martínez, E. Navarro, E. Román, M. García-Hernandez, A. Espinosa, C. Ballesteros, R. Fermento, Y. Huttel, Matrix and interaction effects on the magnetic properties of Co nanoparticles embedded in gold and vanadium, Phys. Chem. Chem. Phys. 15 (2013) 316–329.

[63] L. Bossard-Giannesini, H. Cruguel, E. Lacaze, O. Pluchery, Plasmonic

properties of gold nanoparticles on silicon substrates: Understanding Fano-like spectra observed in reflection, Appl. Phys. Lett. 109 (2016) 111901.
[64] C. Humbert, O. Pluchery, E. Lacaze, B. Busson, A. Tadjeddine, Two-Colour Sum-Frequency Generation Spectroscopy Coupled to Plasmonics with the CLIO Free Electron Laser, Photonics 9 (2022) 55.
[65] B. Bourguignon, W. Zheng, S. Carrez, A. Ouvrard, F. Fournier, H. Dubost, Deriving the complete molecular conformation of self-assembled alkanethiol molecules from sum-frequency generation vibrational spectra, Phys. Rev. B 79 (2009) 125433.
[66] M. Himmelhaus, F. Eisert, M. Buck, M. Grunze, Self-Assembly of *n*-Alkanethiol Monolayers. A Study by IR–Visible Sum Frequency Spectroscopy (SFG), J. Phys. Chem. B 104 (2000) 576–584.
[67] L. Dreesen, C. Humbert, M. Celebi, J. J. Lemaire, A. A. Mani, P. A. Thiry, A. Peremans, Influence of the metal electronic properties on the sum-frequency generation spectra of dodecanethiol self-assembled monolayers on Pt(111), Ag(111) and Au(111) single crystals, Appl. Phys. B 74 (2002) 621–625.
[68] L. Dalstein, A. Revel, C. Humbert, B. Busson, Nonlinear Optical Response of a Gold Surface in the Visible Range: A Study by Two-Color Sum-Frequency Generation Spectroscopy. I. Experimental Determination, J. Chem. Phys. 148 (2018) 134701.
[69] J. D. C. Jacob, S. Rittikulsittichai, T. R. Lee, S. Baldelli, Characterization of SAMs Derived from Octadecyloxyphenylethane-thiols by Sum Frequency Generation, J. Phys. Chem. C 117 (2013) 9355–9365.
[70] J .D. C. Jacob, T. R. Lee, S. Baldelli, In Situ Vibrational Study of the Reductive Desorption of Alkanethiol Monolayers on Gold by Sum Frequency Generation Spectroscopy, J. Phys. Chem. C 118 (2014) 29126–29134.
[71] N. Nishi, D. Hobara, M. Yamamoto, T. Kakiuchi, Chain-length-dependent change in the structure of self-assembled monolayers of n-alkanethiols on Au(111) probed by broad-bandwidth sum frequency generation spectroscopy, J. Chem. Phys. 118 (2003) 1904–1911.
[72] R. G. Nuzzo, L. H. Dubois, D. L. Allara, Fundamental studies of microscopic wetting on organic surfaces. 1. Formation and structural characterization of a self-consistent series of polyfunctional organic monolayers, J. Am. Chem. Soc. 112 (1990) 558–569.
[73] P. E. Laibinis, G. M. Whitesides, D. L. Allara, Y. T. Tao, A. N. Parikh, R. G. Nuzzo, Comparison of the structures and wetting properties of self-assembled monolayers of n-alkanethiols on the coinage metal surfaces, copper, silver, and gold, J. Am. Chem. Soc. 113 (1991) 7152–7167.
[74] F. Schreiber, Structure and growth of self-assembling monolayers, Prog. Surf. Sci. 65 (2000) 151–257.
[75] C. Du, R. S. Andino, M. C. Rotondaro, S. W. Devlin, S. Erramilli, L. D. Ziegler, M. M. Thuo, Substrate Roughness and Tilt Angle Dependence of Sum-Frequency Generation Odd–Even Effects in Self-Assembled Monolayers, J. Phys. Chem. C 126 (2022) 7294–7306.
[76] J. C. Love, L. A. Estroff, J. K. Kriebel, R. G. Nuzzo, G. M. Whitesides, Self-Assembled Monolayers of Thiolates on Metals as a Form of Nanotechnology, Chem. Rev. 105 (2005) 1103–1170.
[77] C. Noguez, Surface Plasmons on Metal Nanoparticles: The Influence of Shape and Physical Environment, J. Phys. Chem. C 111 (2007) 3806–3819.
[78] B. Busson, L. Dalstein, Sum-Frequency Spectroscopy Amplified by Plasmonics: The Small Particle Case, J. Phys. Chem. C 123 (2019) 26597–26607.
[79] A. Badia, L. Cuccia, L. Demers, F. Morin, R. B. Lennox, Structure and Dynamics in Alkanethiolate Monolayers Self-Assembled on Gold Nanoparticles: A DSC, FT-IR, and Deuterium NMR Study, J. Am. Chem. Soc. 119 (1997) 2682–2692.
[80] M. J. Hostetler, J. J. Stokes, R. W. Murray, Infrared Spectroscopy of Three-Dimensional Self-Assembled Monolayers: N–Alkanethiolate Monolayers on Gold Cluster Compounds, Langmuir 12 (1996) 3604–3612.